RSC Advances

PAPER

View Article Online
View Journal | View Issue

Cite this: *RSC Adv.*, 2020, **10**, 15163

Synergistic effect of potassium iodide and sodium dodecyl sulfonate on the corrosion inhibition of carbon steel in HCl medium: a combined experimental and theoretical investigation

Jianhong Tan,[a] Lei Guo, *[b] Hong Yang,[b] Fan Zhang[c] and Youness El Bakri[d]

Carbon steel is an important industrial material, but it usually suffers from serious corrosion in the service environment. Using corrosion inhibitors is an effective approach to mitigate corrosion. The synergistic inhibition behavior of sodium dodecyl sulfonate (SDS) and potassium iodide (KI) on carbon steel corrosion in hydrochloric acid medium was investigated by electrochemical test, surface morphology analysis, and molecular simulation approaches. Results show that the corrosion inhibition performance is significantly enhanced after the two substances are compounded, and the inhibition efficiency can reach approximately 96% at small doses. The Tafel polarization curves suggest that the mixtures can be classified as anodic corrosion inhibitors. Impedance tests indicate that the inhibitor molecules are adsorbed on the steel surface, resulting in an increase of charge transfer resistance but a decrease of electric double layer capacitance. The adsorption process follows the Langmuir adsorption isotherm. Molecular simulation calculations further reveal the active sites of SDS and the stabilizing effect that I^- plays in the inhibition process. The present research offers an economic, environmentally friendly and efficient measure of corrosion control, and provides theoretical guidance for the efficient use of carbon steels and the development of novel corrosion inhibitors.

Received 2nd March 2020
Accepted 12th April 2020

DOI: 10.1039/d0ra02011g

rsc.li/rsc-advances

1. Introduction

Nowadays, carbon steels are important industrial materials because they are cost effective, readily available, and have excellent mechanical properties. They are widely used in construction, transportation, medicine, fire protection and other fields. In particular, they are the main raw materials of pickling equipment. However when the steels are exposed to the acidic environments, they may undergo serious degradation, which leads to a number of inevitable accidents, huge economic losses and safety considerations.[1] There is extensive literature indicating that the use of corrosion inhibitors is an important approach to inhibit metal corrosion.[2–4] Generally, organic molecules containing hetero atoms (O, S, N), unsaturated bonds, π-electrons or polar functional groups can be expected to be excellent corrosion inhibitors.[5–7] Many compounds such as plant extracts, drugs, and synthetic organic molecules have been proven to have good corrosion inhibition effects.[8,9] It is generally believed that these inhibitor molecules protect the metal by adsorption on the substrate surface through donor–acceptor interactions.[10] Some scholars have confirmed that multi-active compounds with large molecular volume tend to have better inhibition performance.[11–13] However, there are still huge challenges in chemically synthesizing such inhibitors. Moreover, it is also an important approach to enhance the corrosion inhibition efficiency by using the synergistic effect between the inhibitor molecules and other additives.[14,15] It is reported that ionic liquids with long alkyl chains can be served as effective corrosion inhibitors.[16,17] Interestingly, as depicted in Fig. 1, researchers have found that their excellent inhibition performance is mainly due to the inherent synergistic corrosion inhibition effect between anions and cations.[18] Unfortunately, most of the current research on ionic liquid-based inhibitors is still in the laboratory development stage, and there are not many industrial applications. The main reasons include the following aspects: price, solubility limit, stability, biodegradability of the inhibitors.[19] Especially the price factor is particularly important. Overall, challenges remain in developing high-quality and cost-effective composite inhibitors. This drove us to seek an ionic liquid analog, such as a mixture of sodium dodecyl sulfonate and KI, which simultaneously contains polar alkyl chain and anion with strong adsorption characteristics.

[a]School of Chemistry and Chemical Engineering, Yangtze Normal University, Chongqing 408100, China
[b]School of Material and Chemical Engineering, Tongren University, Tongren 554300, China. E-mail: cqglei@163.com
[c]Division of Surface and Corrosion Science, Department of Chemistry, KTH Royal Institute of Technology, Stockholm SE-10044, Sweden
[d]South Ural State University, Lenin Prospect 76, Chelyabinsk, 454080, Russian Federation

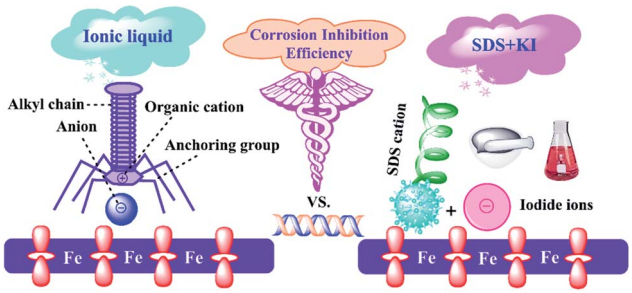

Fig. 1 A comparison diagram for the corrosion inhibition performance of common ionic liquid and SDS&KI.

The objective of this work is to ascertain the synergistic effect of KI and SDS as corrosion inhibitor components for carbon steel in 1 M HCl solution. Electrochemical methods, surface morphological analysis, and contact angle techniques were used to explore the anti-corrosion performance. In addition, density functional theory (DFT) and molecular dynamics (MD) simulation were further employed to provide molecular level insights into the inhibition mechanism.

2. Materials and methods

2.1 Materials preparation

The chemical composition of carbon steel used is as follows: Mn (0.13%), Si (0.18%), S (0.04%), C (0.17%), P (0.04%) and the balance Fe. The steel block with dimensions 1 cm × 1 cm × 1 cm was prepared to used as working electrodes, and its five sides were sealed with epoxy resin leaving a 1 × 1 cm^2 contact area. The electrodes were abraded successively by different sizes of sandpaper (400, 600, 800, 1000, 1200 mesh) before each experiment. Then they were degreased with ethyl alcohol and dried at room temperature for use. SDS and KI were purchased from Sigma-Aldrich. The aggressive medium, *i.e.*, 1 M HCl, was prepared using ultrapure water and analytical reagent grade 37% HCl. The H_2SO_4 without DDA was treated as blank for comparison. The selected concentrations of SDS were 0.1, 0.5, 1.0, and 5.0 mM, while a fixed concentration (5.0 mM) was adopted for KI to explore the effects of iodide ions.

2.2 Electrochemical tests

Electrochemical experiments were carried out on the RST5000 electrochemical workstation with a conventional three-electrode system. The working electrode was the prepared carbon steel, the reference electrode was saturated calomel electrode (SCE) equipping with a vitreous Luggin capillary to reduce solution impedance, and the counter electrode was a platinum foil. The potentials obtained from all electrochemical tests were based on SCE. Initially, the steel electrode was kept dipped in the tested solution for 1 h to attain a steady open circuit potential (E_{OCP}). Afterwards, electrochemical impedance spectroscopy (EIS) test was measured within 10 mHz to 100 kHz frequency range using ±10 mV alternating current signal at E_{OCP}. The obtained impedance data were analyzed applying the ZsimpWin (version 3.6) software, which exploits simple and efficient Down-Hill simplex method instead of popular Marquardt transformation during the fitting procedure. Then potentiodynamic polarization measurements were performed by sweeping the potential from ±250 mV *vs.* E_{OCP} at 0.0167 mV s^{-1}. Each experiment was repeated three times to reduce errors and the temperature was thermostatically controlled at 298 K.

2.3 Surface characterization

The carbon steel surface was studied by immersing the metallic samples in 1 M HCl without and with optimal concentration of inhibitor for 4 h. After removing the samples from the test solution, the specimens were subsequently washed by absolute ethanol and ultrapure water, then dried in air. The surface morphology of carbon steel was observed using a JEOL-JSM-7800F model scanning electron microscopy (SEM, voltage 15 kV) equipped with energy dispersive spectroscopy (EDS) detector at high vacuum. The water static contact angles (CA) of the steel surface were measured by a CA meter (XG-CAMB, XuanYi Instrument Ltd., China). The values were recorded five times at different positions and the mean value was selected as a final value.

2.4 Computational details

All calculations were performed using Material Studio (MS) software (version 8.0).[20] DFT calculations were performed by

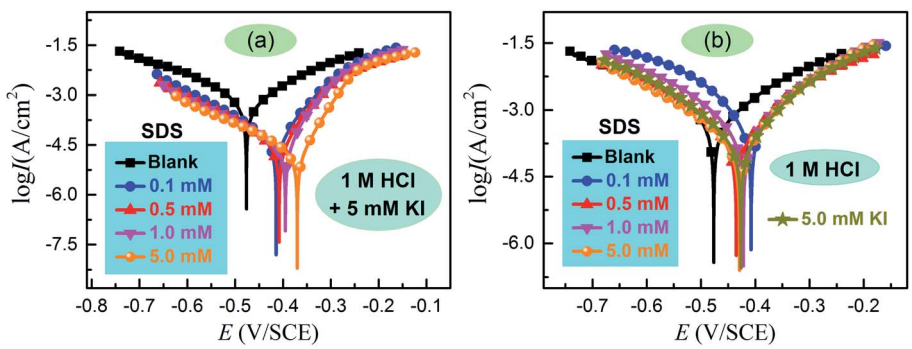

Fig. 2 Potentiodynamic polarization behavior of carbon steel in 1 M HCl with (a) associative and (b) individual inhibitors.

Dmol3 module, employing the GGA-BLYP exchange-correlation functional and double numeric quality with polarization (DNP) basis set. The effect of solvent was addressed by using COSMO implicit model (H_2O, dielectric constant 78.54).[21] The convergence thresholds for energy, maximum force, and maximum atomic displacement were of 1×10^{-5} Ha, 2×10^{-3} Ha Å^{-1}, and 5×10^{-3} Å, respectively. The adsorption behavior of inhibitor molecules on carbon steel surface was investigated using the Forcite mode. The simulation was conducted in a 14.8 × 14.8 × 38.1 Å simulation box with periodic boundary conditions, which consisted of a Fe(110) slab and a solvent layer (with $300H_2O$ + 1SDS + $20I^-$). Fe(110) plane was chosen due to its highly stabilized and packed structure. The COMPASSII force field was adopted, which is an *ab initio* force field, and its nonbond interaction energy is given by the following equation:[22]

$$E_{\text{nonbond}} = \sum_{i,j} \varepsilon_{ij} \left[2\left(\frac{r_{ij}^0}{r_{ij}}\right)^9 - 3\left(\frac{r_{ij}^0}{r_{ij}}\right)^6 \right] + \sum_{i,j} \frac{q_i q_j}{r_{ij}} \quad (1)$$

where q_i and q_j are the charges of i and j atoms, ε_{ij}, r_{ij}^0, and r_{ij} represent the energy parameter, dimension parameter, and the distance between particles i and j, respectively. The whole system was performed under Andersen thermostat, NVT ensemble, with a time step of 1.0 fs and simulation time of 1000 ps. Non-bond interactions, van der Waals and electrostatic, were set as atom-based summation method and Ewald summation method, respectively, with a cutoff radius of 1.55 nm.

3. Results and discussion

3.1 Potentiodynamic polarization measurement

Fig. 2 shows the typical potentiodynamic polarization curves for carbon steel in 1 M HCl, both in the presence and absence of associative and individual SDS/KI inhibitors. The results showed that in all cases the inhibitors can restrain both the anodic dissolution of carbon steel as well as the hydrogen evolution reaction, which may be attributed to the adsorption of inhibitor molecules on the active sites of steel substrate.[23] It is obvious that the combinations of SDS and KI, produce pronounced effects on the corrosion current density compared to those displayed by individual KI or SDS. This behavior suggests that SDS and KI have a synergistic effect in inhibiting the corrosion of carbon steel in HCl solution. Several polarization parameters including corrosion potential (E_{corr}), corrosion current density (I_{corr}), anodic and cathodic Tafel slopes (β_a and β_c) were deduced by Tafel extrapolation method. The corresponding inhibition efficiency was calculated by the following equation:[24]

$$\eta_P\% = \frac{I_{\text{corr},0} - I_{\text{corr}}}{I_{\text{corr},0}} \times 100 \quad (2)$$

where $I_{\text{corr},0}$ and I_{corr} represent uninhibited and inhibited corrosion current densities, respectively. The obtained values are summarized in Table 1. It is not difficult to find that the I_{corr} values substantially decrease with increase in SDS concentration. Moreover, the addition of 5 mM KI shifted E_{corr} positively

Table 1 Polarization parameters of carbon steel in 1 M HCl containing different concentrations of SDS in the presence and absence of KI

C_{SDS} (mM)	C_{KI} (mM)	E_{corr} (V/SCE)	I_{corr} (μA cm^{-2})	$-\beta_c$ (mV dec^{-1})	β_a (mV dec^{-1})	η_P (%)	S_P
Blank	—	−0.476	574.9	133.2	112.4	—	—
Blank	5.0	−0.426	139.3	100.1	83.2	75.7	—
0.1	—	−0.407	321.3	85.8	97.1	44.1	—
0.1	5.0	−0.414	41.1	112.8	62.5	92.8	1.886
0.5	—	−0.421	263.9	102.3	92.1	54.1	—
0.5	5.0	−0.408	30.7	118.3	57.8	94.6	2.065
1.0	—	−0.434	193.1	108.8	93.6	66.4	—
1.0	5.0	−0.394	25.3	124.8	46.6	95.5	1.814
5.0	—	−0.429	179.3	110.8	76.5	68.8	—
5.0	5.0	−0.370	17.7	136.7	47.2	96.9	2.445

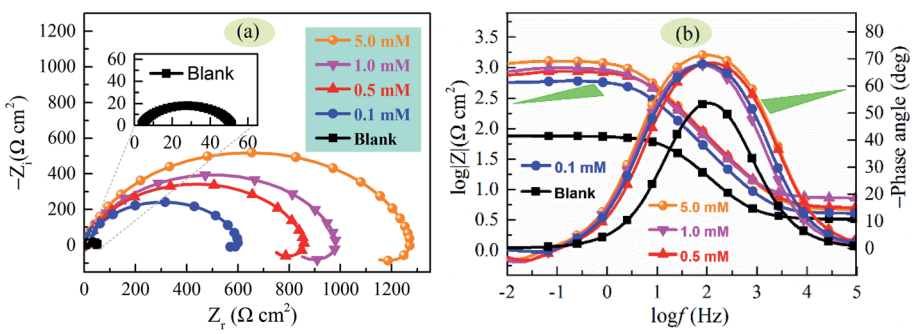

Fig. 3 (a) Nyquist and (b) Bode plots for carbon steel in 1 M HCl + 5 mM KI solution with various concentrations of SDS.

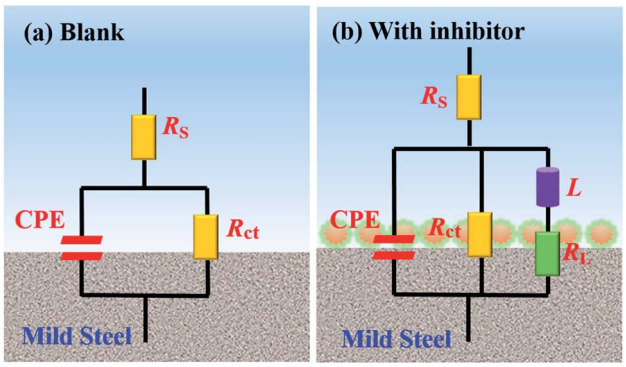

Fig. 4 Equivalent circuits used to fit the EIS data for carbon steel in 1 M HCl (a) without and (b) with inhibitor.

and further reduced the corrosion current density, thereby significantly enhanced the inhibition efficiency. It is generally recognized that the iodide ions adsorbed on the steel surface facilitated the adsorption of SDS by means of the electrostatic interaction which led to the high inhibition efficiency.[25] According to data of Table 1, the optimal corrosion inhibition efficiency is 96.9%, when the mixture is 5 mM SDS + 5 mM KI. In this circumstance, the E_{corr} displacement is greater than 85 mV with respect to the blank, which suggests that the mixture can be considered as anodic inhibitors.[26] This can be confirmed by the changes of β_c and β_a values, indicating that the anodic reactions are more obviously affected than cathodic reactions by the presence and concentration of studied inhibitor.

3.2 EIS measurement

Nyquist and Bode plots of carbon steel in 1 M HCl solution containing different concentrations of SDS in the presence of 5 mM KI are presented in Fig. 3. As can be seen from Fig. 3a, for the inhibited cases, all the Nyquist diagrams consist of a capacitive loop at high frequencies and a small inductive loop at low frequencies. The high frequency capacitive loop is usually related to the time constant of charge transfer of the corrosion process and double layer behavior, while the low frequency inductive loop can be attributed to the relaxation process obtained by adsorption species like $(Cl^-)_{ads}$ and $(H^+)_{ads}$ or adsorption–desorption process of inhibitor species on the electrode surface.[27] Furthermore, the diameter of capacitive loop as well as the values of phase angle and impedance magnitude ($|Z|$) (see Fig. 3b) significantly increases with increasing inhibitor concentration, indicating better protection of inhibitor with higher concentrations. Moreover, only one time constant is found in the Bode format, suggesting that the corrosion process of carbon steel in test solution is mainly charge-transfer controlled.

The designed equivalent circuit for impedance data fitting is represented in Fig. 4, where R_s stands for the solution resistance, R_{ct} represents the charge transfer resistance, R_L and L are the inductive elements. CPE is the constant phase element, which is usually used to provide a more accurate fitting result instead of a pure capacitor. The impedance function of CPE is defined as:[28]

$$Z_{CPE} = Y_0^{-1}(j\omega)^{-n} \quad (3)$$

where Y_0 is the magnitude of CPE, ω is the angular frequency, $j^2 = -1$ means the imaginary number, and n denotes the index of surface irregularity ($-1 \le n \le +1$). When $n = 0$, -1, and 1, CPE stand for resistor, inductor, and pure capacitor, respectively. The double layer capacitance (C_{dl}) and inhibition efficiency (η_E) were determined according to the relations given below:[29]

$$C_{dl} = Y_0(\omega_{max})^{n-1} = Y_0(2\pi f_{Z_{im}-max})^{n-1} \quad (4)$$

$$\eta_E\% = \frac{R_{ct} - R_{ct,0}}{R_{ct}} \times 100 \quad (5)$$

where ω_{max} implies the frequency at which the imaginary impedance in the Nyquist plot is maximum. $R_{ct,0}$ and R_{ct} are the charge transfer resistances in the absence and presence of inhibitors, respectively. In our work, the measure of goodness of EIS fit to model is χ^2 parameter, defined as:[30]

$$\chi^2 = \sum_{i=1}^{n}\left[\frac{\left(Z_i'\left(\omega_i, \vec{p}\right) - a_i\right)^2}{a_i^2 + b_i^2} + \frac{\left(Z_i''\left(\omega_i, \vec{p}\right) - b_i\right)^2}{a_i^2 + b_i^2}\right] \quad (6)$$

where ω_i, a_i, b_i are experimental data points, $\vec{p}$ is a parameter associated with a model, and Z_i' and Z_i'' are calculated points.

Table 2 Electrochemical impedance parameters for carbon steel in 1 M HCl at different concentrations of SDS in the presence and absence of 5 mM KI

C_{SDS} (mM)	C_{KI} (mM)	R_s (Ω cm^2)	Y_0 ($\times 10^{-6}$ S s^n cm^{-2})	n	C_{dl} (μF cm^{-2})	R_L (Ω cm^2)	L (H cm^2)	R_{ct} (Ω cm^2)	η(%)	χ^2 ($\times 10^{-4}$)	S_E
Blank	—	3.86	304.7	0.823	283.1			47.6	—	8.23	—
Blank	5.0	3.47	112.8	0.844	166.1	4.5	37.4	234.5	79.7	9.38	—
0.1	—	3.25	338.8	0.826	378.7	3.6	30.9	84.9	43.9	9.67	—
0.1	5.0	3.98	89.8	0.853	77.9	9.7	89.6	609.5	92.1	8.98	1.441
0.5	—	4.02	315.1	0.823	339.4	6.8	70.8	114.2	58.3	9.54	—
0.5	0.5	4.95	53.4	0.852	48.5	14.8	126.4	864.6	94.4	9.59	1.511
1.0	—	3.78	243.4	0.826	276.4	10.9	108.9	151.6	68.6	8.97	—
1.0	1.0	4.69	51.6	0.856	45.7	27.9	274.3	989.3	95.1	9.44	1.301
5.0	—	4.62	278.5	0.824	298.6	15.7	220.6	156.1	69.5	6.38	—
5.0	5.0	4.61	48.6	0.867	43.5	34.8	378.9	1281.1	96.2	9.39	1.629

The derived impedance parameters are recorded in Table 2. We can see that the χ^2 values are fairly small ($<1 \times 10^{-3}$), suggesting high fit of received impedance spectra to proposed equivalent circuits. The values of both R_{ct} and η_E are found to increase by increasing the inhibitor concentration, while the values of C_{dl} appear a downward trend. The decrease in C_{dl} may result from a decrease in local dielectric constant and/or an increase in the thickness of the electrical double layer, which can be explained in terms of the Helmholtz model:[31]

$$C_{dl} = \frac{\varepsilon^0 \varepsilon}{d} A \quad (7)$$

where ε and ε^0 show the dielectric constant for the vacuum and the relative permittivity, respectively. A is the surface area of the steel electrode, and d stands for the thickness of the electric double layer. There existed a gradual replacement process of water molecules and other ions that were originally adsorbed on the electrode surface during adsorption of inhibitor molecules on the steel surface. This replacement process eventually led to the reduction in C_{dl}. The addition of 5 mM KI further enhances the R_{ct} values and reduces the C_{dl} values. This can be attributed to the enhanced adsorption of SDS in the presence of KI on account of the synergistic effect of iodide ions. Our EIS findings confirm the reliability of potentiodynamic polarization measurements.

3.3 Adsorption isotherm and synergistic effect

To further cognize the adsorption behavior of inhibitor molecules on the metal surface, some frequently used adsorption isotherms have been tested to explore the mechanisms. As displayed in Fig. 5, the successful fitting of the C/θ *vs.* C plot indicates that the inhibitor adsorption obeys the Langmuir adsorption isotherm, which can be presented as follows:[32,33]

$$\frac{C}{\theta} = \frac{\theta}{K_{ads}} + C \quad (8)$$

where C is the concentration of inhibitor, K_{ads} denotes the adsorption equilibrium constant, θ symbolizes the surface coverage obtained from the EIS measurements, approximately equaling to corrosion inhibition efficiency. The linear regressive coefficient ($R^2 = 0.9999$) indicates that the fitting result is reliable. According to the slope value, the equilibrium adsorption constant (K_{ads}) was calculated, which is related to adsorption Gibbs free energy (ΔG_{ads}):[34]

$$\Delta G_{ads} = -RT \ln(55.5 K_{ads}) \quad (9)$$

where 55.5 is the concentration of water in the test solution denoted in mol L^{-1}. The computed K_{ads} and ΔG_{ads} values were 1.02×10^5 L mol^{-1} and -38.5 kJ mol^{-1}, respectively. From this we infer that the adsorption of SDS and iodide ions on the steel substrate can occur spontaneously. Generally, values of ΔG_{ads} up to -20 kJ mol^{-1} are considered as physisorption, whereas those around -40 kJ mol^{-1} or lower are related to chemisorption, which involves electronic sharing and/or transfer between organic inhibitors and metal surface to form coordinate-type bonds.[35] The obtained ΔG_{ads} value in this work are in the range of -40 to -30 kJ mol^{-1}, indicating that the adsorption mechanism of SDS and KI on carbon steel in 1 M HCl solution belongs to a combined type of physisorption and chemisorption, with the latter as the dominant. The synergistic inhibition effect of inhibitors takes place when the total action of compounds is higher than the sum of each one individually.

Moreover, to further verify the synergistic effect, a descriptor synergism parameter (S) was introduced and calculated, which was defined as:[36]

$$S = \frac{1 - (\theta_1 + \theta_2) + (\theta_1 \theta_2)}{1 - \theta_{1+2}} \quad (10)$$

where θ_1, θ_2, and θ_{1+2} are the surface coverage values by single KI, SDS, and their combinations, respectively. Generally, in the case where the SDS and KI inhibitors have no effect on each other and adsorb on the steel–solution interface independently, $S = 1$. Otherwise, synergistic effects manifest if $S > 1$, and antagonistic effects when $S < 1$.[37] As given in Tables 1 and 2, all the S values (S_P and S_E) are greater than 1, confirming the synergistic action of iodide ions with SDS.

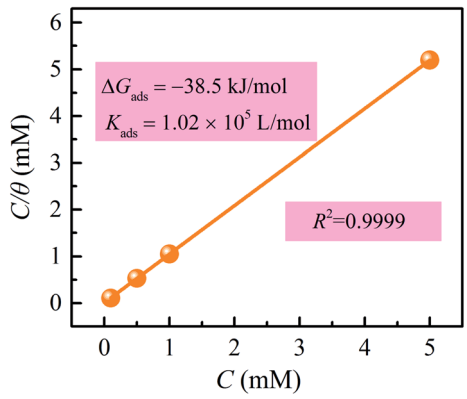

Fig. 5 Langmuir isotherm plot for the adsorption of SDS and KI on carbon steel.

3.4 SEM and contact angle analyses

To directly observe the protective effect of investigated inhibitors, the morphology of carbon steel surface submerged in 1 M HCl without and with 5 mM (SDS + KI) was checked using SEM. As to the blank condition (Fig. 6a), we can find that the surface is very rough, corroded and irregular. The corrosive solution attacked the steel surface and the steel formed rust after corroding. Fig. 6c gives the morphology of steel specimen treated with the inhibitors. Obviously, the entire surface is flat and rarely eroded, indicating that the presence of SDS and KI blocked the active sites of the steel surface and inhibited the corrosion progression. Besides, EDS survey spectra were also carried out to detect which elements were present or disappeared on the steel surface before and after the addition of inhibitors to the solution. It can be seen from Fig. 6b that the corrosion products, depositing on the surface of carbon steel, may mainly be composed of iron oxides under inhibitor-free conditions. Conversely, in the inhibited system, several additional signals such as S and I were observed from Fig. 6d, and

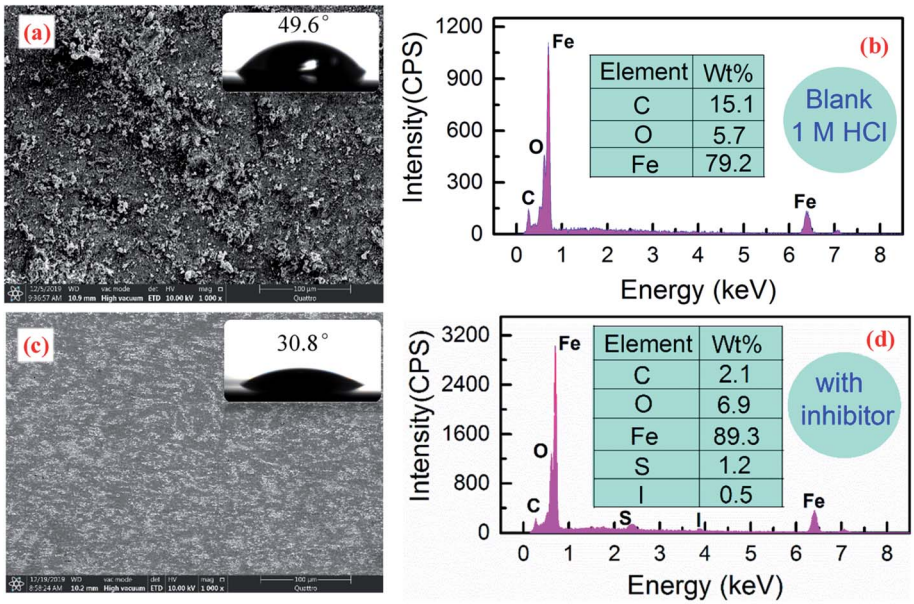

Fig. 6 SEM-EDS analysis for carbon steel samples immersed in 1 M HCl (a and b) without and (c and d) with 5 mM (SDS + KI). The insets are water contact angles on the corresponding surfaces.

the increase of Fe content indicates that the inhibitor molecules prevent the dissolution of iron. The measured contact angles for the carbon steel surface in the absence and presence of inhibitors are 49.6° and 30.8°, respectively. The former has a relatively high value may be due to the formation of polar inorganic corrosion products on the steel surface, thus decreasing its wettability. While in the inhibited condition, there are less corrosion products, and the presence of potassium iodide increases the wettability of the steel surface and therefore exhibits a smaller contact angle value.

3.5 Theoretical considerations

Normally, the active sites of inhibitors can be elucidated by frontier molecular orbital theory. Thus, DFT calculations were performed in this work to investigate the relationship between molecular structure and corrosion inhibition performance. The optimized molecular structure, frontier molecule orbitals (HOMO, LUMO) and electrostatic potential (ESP) distributions of SDS anion are shown in Fig. 7a–d. Analysis of Fig. 7b and c shows that the distributions of HOMO and LUMO mainly locate on the atoms of sulfonic group, consequently these are the favorite sites for interaction with the steel surface. This can be further confirmed by the ESP diagram. As displayed in Fig. 7d, the red area denotes nucleophilicity while the blue region means electrophilicity.[38] The red regions are mostly concentrated on S and O atoms, which are more likely to form covalent bonds with Fe 3d orbitals.

Furthermore, MD simulation was implemented to get additional evidence about the interaction between inhibitor molecule and iron surface. We have ensured that the whole system reached equilibrium until both temperature and energy were balanced. The equilibrium configuration (top and side views) of Fe(110)/I^-/SDS/H_2O adsorption system is shown in Fig. 7e. We can see that iodine ions are tightly attached to the steel substrate. As to SDS, the polar sulfonic acid group is connected

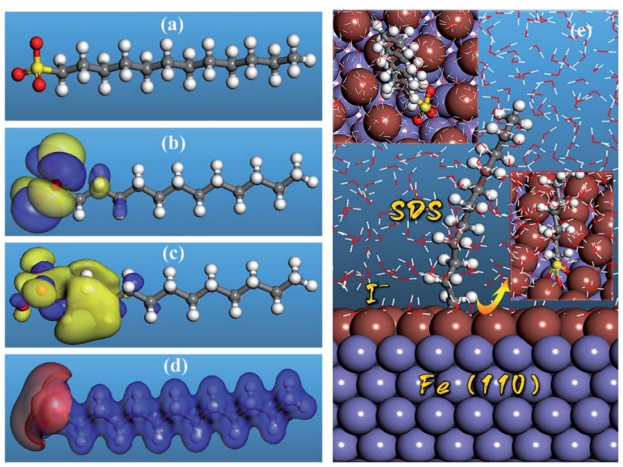

Fig. 7 (a) Optimized structure, (b) HOMO, (c) LUMO, and (d) ESP of SDS anion, (e) the most stable low energy configuration of the Fe(110)/I^-/SDS/H_2O adsorption system.

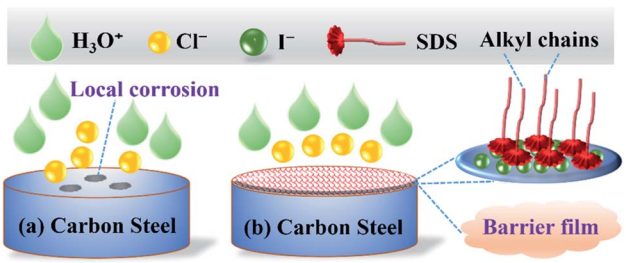

Fig. 8 Schematic illustrations for the anticorrosive mechanism of KI and SDS in (a) uninhibited and (b) inhibited HCl media.

Table 3 Comparison with other ionic liquid based corrosion inhibitors

Inhibitor	System	Optimum concentration	Inhibition efficiency	Average cost	Ref.
SDS + KI	Carbon steel/1 M HCl	5 mM	96.7%	3 CNY per g	This work
1-Vinyl-3-methylimidazolium iodide	X70 steel/0.5 M H_2SO_4	5 mM	96.0%	318 CNY per g	18
N^1,N^1,N^1,N^2,N^2,N^2-Hexadodecylhexane-1,6-diaminium bromide	Carbon steel/1 M HCl	5 mM	94.0%	Unattainable	42
1-Allyl-3-octylimidazolium bromide	Mild steel/0.5 M H_2SO_4	10 mM	93.0%	57 CNY per g	44

to the iron atoms and iodine ions, while the long alkyl chain is placed in the solution. We can deduce that a self-assembled hydrophobic barrier may be formed to protect steel from corrosion. The adsorption energy can be quantitatively evaluated according to the following equation:[39]

$$E_{ads} = E_{total} - (E_{surf+solu} + E_{inh+solu}) + E_{solu} \quad (11)$$

wherein, E_{total} denotes the total energy of the whole studied system, $E_{surf+solu}$ is referred to the total energy of Fe(110) surface and solution without the inhibitor, $E_{inh+solu}$ represents the total energy of the inhibitor and solution, and E_{solu} is the total energy of the solution. It is generally assumed that a more negative E_{ads} value suggests a stronger interaction between the adsorbent and the adsorbate. In our work, the calculated negative E_{ads} value (-298.6 kJ mol^{-1}) indicates the stability of simulation system and spontaneous adsorption can be expected.

3.6 Mechanism of adsorption and inhibition

The anticorrosive mechanism of SDS and KI for carbon steel was further clarified. In the uninhibited HCl solution, it is generally assumed that the pitting corrosion reaction of steel can occur according to the following steps:[40]

$$Fe + Cl^- \rightleftharpoons (FeCl)_{ads} + e^- \quad (12)$$

$$(FeCl)_{ads} \rightleftharpoons (FeCl^+) + e^- \quad (13)$$

$$(FeCl^+) \rightleftharpoons Fe^{2+} + Cl^- \quad (14)$$

However, in the presence of KI inhibitor, I^- will replace Cl^- because of its stronger specific adsorption ability.[41] Then under the synergistic effect of SDS and KI, a self-assembled [Fe(0) Fe(II) I^-SDS] barrier film can be formed very quickly on the steel surface (Fig. 8). This thin film is mainly constructed by the physical and/or chemical adsorption interactions between the inhibitor ions and steel surface atoms, which can block the attack of corrosive ions such as H_3O^+ and Cl^-, eventually protecting the carbon steel from corrosion.

3.7 The cost comparison with other inhibitors

Finally, in order to highlight the cost advantage of the SDS&KI mixture, we contrasted it with other ionic liquid-based corrosion inhibitors, and the results are summarized in Table 3. We can see that although its price cost is relatively low, it still shows good corrosion inhibition performance. As reported in ref. 42, some laboratory-synthesized compounds are currently difficult to obtain, so there is still a great challenge for their wide industrial application. However, we still agree with Gökhan Gece's[43] point of view, that is with the advancement of science and technology, the preparation process of organics will become more and more simple, so compounds that currently seem expensive still have great application potential in the field of anticorrosion.

4. Conclusions

The inhibition behavior of SDS and its synergistic effect with KI for carbon steel in 1 M HCl has been fully investigated. Synergistic effects between SDS and KI were observed. The addition of KI to the solution enhanced the inhibition efficiency of SDS significantly. Potentiodynamic polarization measurements showed that the additives act predominately as anodic inhibitors. SEM morphology analysis indicated that the inhibitors formed an excellent protective film on the steel substrate. Adsorption of SDS and KI on the carbon steel surface obeys Langmuir's adsorption isotherm. A combination of both physisorption and chemisorption of the inhibitor molecules on the carbon steel surface was proposed based on the Gibbs free energy value. Our theoretical calculations provide good support to the experimental findings.

Conflicts of interest

There are no conflicts to declare.

Acknowledgements

This research was supported by the National Natural Science Foundation of China (21706195), the Science and Technology Program of Guizhou Province (QKHJC2016-1149), the Guizhou Provincial Department of Education Foundation (QJHKYZ2018-030), and the Student's Platform for Innovation and Entrepreneurship Training Program (20195200501).

References

1 B. Hou, X. Li, X. Ma, C. Du, D. Zhang, M. Zheng, W. Xu, D. Lu and F. Ma, *npj Mater. Degrad.*, 2017, **1**, 4.
2 S. A. Umoren, M. M. Solomon, I. B. Obot and R. K. Suleiman, *J. Ind. Eng. Chem.*, 2019, **76**, 91–115.

3 I. B. Obot, M. M. Solomon, S. A. Umoren, R. Suleiman, M. Elanany, N. M. Alanazi and A. A. Sorour, *J. Ind. Eng. Chem.*, 2019, **79**, 1–18.
4 L. T. Popoola, *Corros. Rev.*, 2019, **37**, 71–102.
5 B. El Ibrahimi, A. Jmiai, L. Bazzi and S. El Issami, *Arabian J. Chem.*, 2020, **13**, 740–771.
6 L. Hamadi, S. Mansouri, K. Oulmi and A. Kareche, *Egypt. J. Pet.*, 2018, **27**, 1157–1165.
7 S. Satpati, S. K. Saha, A. Suhasaria, P. Banerjee and D. Sukul, *RSC Adv.*, 2020, **10**, 9258–9273.
8 A. Singha and M. A. Quraishi, *J. Mater. Environ. Sci.*, 2015, **6**, 224–235.
9 B. E. A. Rani and B. B. J. Basu, *Int. J. Corros.*, 2012, **2012**, 1–15.
10 G. Frankel, J. Mauzeroll, G. Thornton, H. Bluhm, J. Morrison, V. Maurice, T. Rayment, D. Williams, A. Cook, G. Joshi, A. Davenport, S. Gibbon, D. Kramer, M. Acres, M. Tautschnig, H. Habazaki, P. Marcus, D. Shoesmith, C. Wren, T. Majchrowski, R. Lindsay, M. Wood, M. Todorova, J. Scully, F. Renner, A. Kokalj, C. Taylor, S. Virtanen and J. Wharton, *Faraday Discuss.*, 2015, **180**, 205–232.
11 W. Emori, R.-H. Zhang, P. C. Okafor, X.-W. Zheng, T. He, K. Wei, X.-Z. Lin and C.-R. Cheng, *Colloids Surf., A*, 2020, **590**, 124534.
12 S. L. Fu, S. T. Zhang, Q. Xiang, W. Y. Tan, W. P. Li, S. J. Chen and L. Guo, *Int. J. Electrochem. Sci.*, 2019, **14**, 6855–6873.
13 M. S. Khan, B. Lal, L. K. Keong and K. M. Sabil, *Fluid Phase Equilib.*, 2018, **473**, 300–309.
14 M. Ramezanzadeh, G. Bahlakeh, B. Ramezanzadeh and Z. Sanaei, *J. Ind. Eng. Chem.*, 2019, **77**, 323–343.
15 K. Ramya, K. K. Anupama, K. M. Shainy and A. Joseph, *J. Taiwan Inst. Chem. Eng.*, 2016, **58**, 517–527.
16 C. Verma, E. E. Ebenso and M. A. Quraishi, *J. Mol. Liq.*, 2017, **233**, 403–414.
17 S. Yesudass, L. O. Olasunkanmi, I. Bahadur, M. M. Kabanda, I. B. Obot and E. E. Ebenso, *J. Taiwan Inst. Chem. Eng.*, 2016, **64**, 252–268.
18 L. Feng, S. T. Zhang, Y. J. Qiang, S. Y. Xu, B. C. Tan and S. J. Chen, *Mater. Chem. Phys.*, 2018, **215**, 229–241.
19 G. Shama, *Corros. Sci.*, 2012, **60**, 1–2.
20 M. Meunier, *Mol. Simul.*, 2008, **34**, 887–888.
21 A. Klamt and G. Schüürmann, *J. Chem. Soc., Perkin Trans. 2*, 1993, **2**, 799–805.
22 H. Sun, Z. Jin, C. Yang, R. L. Akkermans, S. H. Robertson, N. A. Spenley, S. Miller and S. M. Todd, *J. Mol. Model.*, 2016, **22**, 47.
23 V. S. Saji, *Corros. Rev.*, 2019, **37**, 187–230.
24 E. McCafferty, *Corros. Sci.*, 2005, **47**, 3202–3215.
25 L. Guo, G. Ye, I. B. Obot, X. Li, X. Shen, W. Shi and X. Zheng, *Int. J. Electrochem. Sci.*, 2017, **12**, 166–177.
26 E. S. Ferreira, C. Giacomelli, F. C. Giacomelli and A. Spinelli, *Mater. Chem. Phys.*, 2004, **83**, 129–134.
27 Y. Li, S. Zhang, Q. Ding, B. Qin and L. Hu, *J. Mol. Liq.*, 2019, **284**, 577–585.
28 G. J. Brug, A. L. G. Vandeneeden, M. Sluytersrehbach and J. H. Sluyters, *J. Electroanal. Chem.*, 1984, **176**, 275–295.
29 M. A. Abu-Dalo, N. A. F. Al-Rawashdeh and A. Ababneh, *Desalination*, 2013, **313**, 105–114.
30 H. Gerengi, *Ind. Eng. Chem. Res.*, 2012, **51**, 12835–12843.
31 J. Haque, V. Srivastava, D. S. Chauhan, H. Lgaz and M. A. Quraishi, *ACS Omega*, 2018, **3**, 5654–5668.
32 A. Mittal, L. Kurup and J. Mittal, *J. Hazard. Mater.*, 2007, **146**, 243–248.
33 K. Y. Foo and B. H. Hameed, *Chem. Eng. J.*, 2010, **156**, 2–10.
34 L. Guo, J. Tan, S. Kaya, S. Leng, Q. Li and F. Zhang, *J. Colloid Interface Sci.*, 2020, **570**, 116–124.
35 K. R. Ansari and M. A. Quraishi, *J. Ind. Eng. Chem.*, 2014, **20**, 2819–2829.
36 Z. Zhang, H. Ba, Z. Wu and Y. Zhu, *Constr. Build. Mater.*, 2019, **198**, 288–298.
37 M. Mobin, R. Aslam and J. Aslam, *Mater. Chem. Phys.*, 2019, **223**, 623–633.
38 P. Politzer and J. S. Murray, *Theor. Chem. Acc.*, 2002, **108**, 134–142.
39 J. Tan, L. Guo, D. Wu, R. Yu, F. Zhang and S. J. I. J. E. S. Kaya, *Int. J. Electrochem. Sci.*, 2020, **15**, 1893–1903.
40 R. Solmaz, G. Kardas, M. Culha, B. Yazici and M. Erbil, *Electrochim. Acta*, 2008, **53**, 5941–5952.
41 L. Guo, Y. Ou, X. Shen, S. Kaya, W. Shi, R. Zhang, X. Zheng and J. Wang, *Int. J. Electrochem. Sci.*, 2017, **12**, 7064–7074.
42 S. M. Tawfik, *J. Mol. Liq.*, 2016, **216**, 624–635.
43 G. Gece, *Corros. Sci.*, 2012, **60**, 3.
44 X. Zheng, S. Zhang, W. Li, M. Gong and L. Yin, *Corros. Sci.*, 2015, **95**, 168–179.

